frontiers | Frontiers in Materials

TYPE Original Research
PUBLISHED 27 April 2023
DOI 10.3389/fmats.2023.1186789

OPEN ACCESS

EDITED BY
Facundo Almeraya-Calderón,
Autonomous University of Nuevo León, Mexico

REVIEWED BY
Qiao Yanxin,
Jiangsu University of Science and Technology, China
Kamalan Kirubaharan Amirtharaj Mosas,
Alexander Dubcek University in Trencin, Slovakia
José Luis Tristancho Reyes,
Technological University of Pereira, Colombia

*CORRESPONDENCE
Dapeng Zhou,
juelichzhou@gmail.com
Yongxin Wang,
wangyongxin@nimte.ac.cn

RECEIVED 15 March 2023
ACCEPTED 17 April 2023
PUBLISHED 27 April 2023

CITATION
Yu M, Zhou D, Zhu B, Cui T, Lu Y and Wang Y (2023), NaCl-induced hot corrosion behaviors of NiSiAlY coatings. *Front. Mater.* 10:1186789. doi: 10.3389/fmats.2023.1186789

NaCl-induced hot corrosion behaviors of NiSiAlY coatings

Miao Yu[1], Dapeng Zhou[2]*, Bing Zhu[1], Tiancheng Cui[2], Yang Lu[1] and Yongxin Wang[2]*

[1]Jilin Provincial Key Laboratory for Numerical Simulation, Jilin Normal University, Jilin, China, [2]Key Laboratory of Marine Materials and Related Technologies, Zhejiang Key Laboratory of Marine Materials and Protective Technologies, Ningbo Institute of Materials Technology and Engineering, Chinese Academy of Sciences, Ningbo, China

In the marine environments, NiCrAlY coatings with high content of Cr would suffer much severer corrosion due to the effect of NaCl. Thus, NiSiAlY coatings with different Si content were proposed and deposited on Ni-based superalloys by multi-arc ion plating. The as-deposited coating was mainly composed of γ′-Ni_3Al phase with a small amount of β-NiAl phase. NaCl-induced hot corrosion tests were performed on the coatings at 500°C, 600°C, and 700°C, respectively. Compared with Ni-based alloy substrates, the NiSiAlY coatings exhibited a good corrosion resistance to NaCl at elevated temperatures. However, with an excessive amount of Si, the NiSiAlY coating showed a degradation in the hot corrosion resistance. In this work, the corrosion mechanisms of the tested coatings were discussed. Moreover, the role of Si was also investigated.

KEYWORDS

NiSiAlY coatings, arc-ion plating, NaCl, hot corrosion, water vapor

1 Introduction

Due to the excellent high-temperature mechanical properties, Ni-based superalloys are widely used for manufacturing aircraft turbine components (Sun et al., 2015; Wu et al., 2019; Wu et al., 2021). Considering the harsh service environments, the thermal components made of Ni-based superalloys are also required to have a good oxidation/hot corrosion resistance (Zhang et al., 2020; Qi et al., 2023). However, to meet the requirement on the mechanical properties, the Ni-based alloys usually make a compromise on the oxidation and corrosion resistance with a relatively low Al and Cr content (Wang et al., 2010; Xing et al., 2014). One practical solution is to apply protective coatings on the surface to improve the corrosion resistance without reducing the mechanical properties of the workpiece itself (Norrell et al., 2020; Yang et al., 2020). Among all the protective coatings, traditional NiCrAlY coatings are widely used due to their excellent oxidation resistance (Wang et al., 2003; Ren et al., 2005; Li et al., 2010; Peng et al., 2013). Generally, the Cr and Al in this coating form dense Cr_2O_3 and Al_2O_3 at a high temperature to protect the inner parts from severe corrosion (Saharkhiz et al., 2020; Texier et al., 2020). In addition, Cr element inside the coating can promote the formation of Al_2O_3.

With the increase of human activities in marine environments, aircraft turbine components face harsh corrosion problems (Gurrappa, 1999; Candan and Bilgic, 2004; Ma et al., 2013). Accordingly, the workpiece has to be subjected to a series of corrosion environments. During service, the solid salt particles along with humid air would be easily sucked into the turbines, depositing on the surface of components (Li et al., 2021). The solid NaCl particles could accelerate the corrosion of the related materials under the synergistic effect of higher temperature air and water vapor (Shu et al., 2000; Wang et al., 2004; Wu et al.,

TABLE 1 Composition of substrates and NiSiAlY targets (wt%).

	Ni	Si	Al	Y	Cr	C	Co	Mo	Ti	Fe
Target 1	Bal	2.5	12	1.5	-	-	-	-	-	-
Target 2	Bal	6.5	12	1.5	-	-	-	-	-	-
Substrate	Bal	-	0.5	-	20	0.06	0.8	3	1	15

2023). Nowadays, researchers showed that the corrosive rate of the Cr-containing alloys can be accelerated by NaCl (Shinata and Nishi, 1986; Wang and Shu, 2003). Cr would produce volatile products, such as $CrCl_3$, which damages the integrity of the protective oxide scale (Sadeghimeresht et al., 2018; Yu et al., 2022). In order to protect the components of the aircraft turbine and prolong the service lifetime, Cr needs to be substituted with new elements. Among the multiple candidate elements, Si is considered as a promising candidate element. Firstly, Si can be well dissolved in Ni-Al binary alloy. Secondly, the Pilling-Bedworth Ratio (PBR) value of Si element is between 1 and 2, Si could thus form a very dense oxide scale during oxidation (Xu and Gao, 2000). Thirdly, Si has excellent chlorination resistance, doping Si in the coatings would help enhance the resistance of alloys to the NaCl-induced hot corrosion (Zhang et al., 2006; He et al., 2013; Hou et al., 2015; Liu et al., 2020). Therefore, to take the advantages of Si, a NiSiAlY coating was proposed in this work.

In this paper, two NiSiAlY coatings named as NiSiAlY Ⅰ (NiSiAlY coatings with 2.5 wt% Si) and NiSiAlY Ⅱ (NiSiAlY coatings with 6.5 wt% Si) were deposited by arc ion plating. The corrosion resistance of the coatings was investigated with NaCl in a humid atmosphere. This paper aimed to investigate the corrosion resistance behavior of the NiSiAlY coatings in a simulated marine service environment, providing some new sight into the protective coating of aero-engine compressor blades.

2 Materials and experimental

2.1 Coating deposition

Ni-based alloy plates (GH4169), as the substrate, were cut into 30*20*3 mm^3 sizes. To reduce the residual stress of the coatings, all the sharp edges of substrates were removed to obtain the chamfers with a 1 mm radius. Two cathode NiSiAlY targets used in this study were supplied by Mat-cn Technology Co., Ltd. (China). The detailed compositions of the used targets and substrates are listed in Table 1.

The NiSiAlY coatings were prepared with a Multi-arc Ion Plating system (MIP, Hauzer Flexicoat 850, Hauzer Techno Coating BV, Netherlands). After being ground with 1,000 grit SiC papers, wet sand-blasted, ultrasonically cleaned, oven dried and cleaned with ethanol and acetone, the substrates were placed in the vacuum chamber. The chamber of the deposition equipment was evacuated to a pressure of about 4×10^{-3} Pa. Then, Ar was introduced into the vacuum chamber as a working gas. Before the deposition, the substrates were subsequently etched by Ar^+ bombardments for 2 min with substrate bias voltages of −900, −1,100, and −1200 V to remove the oxide layers and impurities on the surface. As shown in Table 2, the detailed deposition parameters are presented.

2.2 Experimental procedures

The hot corrosion tests were performed with a hot corrosion testing system as illustrated in Figure 1. It was carried out with a tube furnace (BTF-1200C-Ⅱ, BeQ equipment and technology Co., Ltd., Hefei, China) equipped with a peristaltic pump and a gas flow controller. The dry air was introduced into the well-sealed tube furnace from a compressed air cylinder with a flow rate of 100 sccm. To simulate the humid service environment in the marine environment, deionized water was introduced into heating zone Ⅰ with a flow rate of 0.33 mL/min by the peristaltic pump. Due to the high temperatures, the deionized water can be immediately evaporated into water vapor. Meanwhile, it was carried by airflow to the heating zone Ⅱ where the corrosion tests were performed. Prior to the corrosion tests, solid NaCl particles were applied on the tested samples by spraying an ethanol-based saturated salt solution. After drying by hot air, the deposited solid NaCl on the surface was controlled to a mass of 3 ± 0.15 mg/cm^2. After the furnace achieved the target temperature and stable atmosphere, the samples were quickly loaded into the heating zone. With an interval of 4 h, the tested samples were taken out from the tube furnace, cooling down to room temperature in air. Then, the tested samples were weighted by an electronic scale (EX125DZH, OHAUS, U.S.) with an accuracy of 10^{-5} g. Each sample was weighed three times to get an accurate mass gain. The mass gain during the hot corrosion test can be calculated by the following Eq. 1:

$$\Delta w = (w_t - w_i)/S \quad (1)$$

in where Δw (mg/cm^2) was the mass change per unit area; S represented the surface area of the oxidized sample in cm^2; w_t (mg) was the net mass of the sample with different corrosion

TABLE 2 The deposition parameters of the NiSiAlY coatings.

Process step	Chamber pressure (Pa)	Bias voltage (V)	Temperature (°C)	Arc current (A)	Ar gas flow (sccm)	Time (min)
Bombardment cleaning	0.28	−900	200	60	70	6
		−1,100				
		−1,200				
NiSiAlY	0.60	−100	200	70	400	120

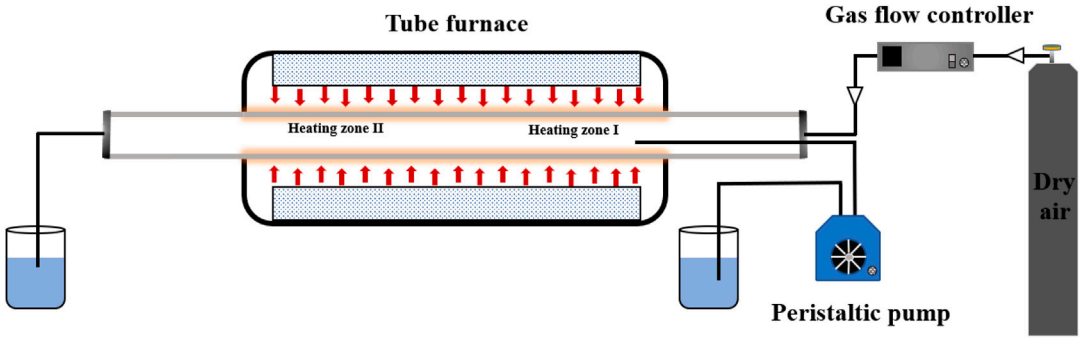

FIGURE 1
Schematic illustration of the hot corrosion testing system.

TABLE 3 Chemical composition of the as-deposited coatings.

	Ni (wt%)	Si (wt%)	Al (wt%)	Y (wt%)
NiSiAlY I	83.8	2.6	11.9	1.7
NiSiAlY II	79.7	6.8	12.1	1.4

time; w_i (mg) was the initial net mass of the sample. After measurement, the coatings were re-coated with fresh NaCl particles and restarted the hot corrosion test.

The surface morphologies of the NiSiAlY coatings before and after corrosion were characterized by the Scanning Electron Microscopy (SEM, EVO18, Carl Zeiss AG, Germany) equipped with an Energy Dispersive Spectrometer (EDS). The microstructural of the coating was characterized by the X-ray diffraction (XRD, D8 ADVANCED DAVICI, Bruker Corporation, Germany) with Cu Kα radiation (λ= 0.154 nm), which was performed as the voltage at 40 kV and the current at 40 mA. The scanning range was set to be 20°–90° with a step size of 0.02°, and the scanning time lasted for 12 min for each sample. Cross-sections of the coatings were prepared by a Focused Ion Beam (FIB, Auriga, Carl Zeiss AG, Germany) equipped with an Energy Dispersive Spectrometer (EDS, AZTEC, Oxford Instrument, The United Kingdom). Before characterization, a Pt film was deposited on the surface of coatings in order to improve the conductivity of coatings. The Photoluminescence (inVia Reflex, Renishaw, United Kingdom) with a spot size of 5.4 μm in diameter was used to determine the type of Al_2O_3 formed during the corrosion test.

3 Results and discussion

3.1 Results

The actual chemical compositions of the as-deposited coatings evaluated by EDS were presented in Table 3. Compared to the components of targets, no significant deviation in the chemical composition was found from the as-deposited coating. As shown in

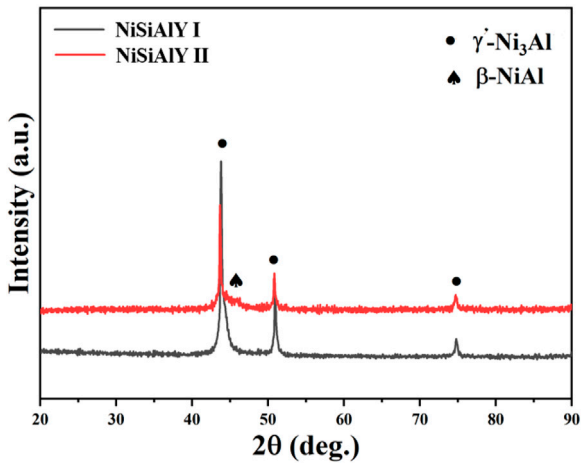

FIGURE 2
XRD patterns of the NiSiAlY coatings.

Figure 2, XRD analysis displayed that both the NiSiAlY coatings mainly consisted of the γ'-Ni_3Al and β-NiAl phases. Moreover, no diffraction peak of silicide was found, indicating that Si was well dissolved in the coatings.

Corrosion kinetic curves of the NiSiAlY coatings during the hot corrosion tests at different temperatures are presented in Figure 3. Moreover, the substrates as the reference were also subjected to corrosion tests. During the corrosion test, the weight loss of both coatings was observed in the initial stage of corrosion at all three temperatures. Moreover, at the lowest test temperature (500°C), the weight of both coatings decreased continuously during the whole corrosion process (Figure 3A). With a low melting point, solid NaCl has a very high evaporation rate in high-temperature environments (Tsaur et al., 2005). Thus, the weight loss could be attributed to that the growth rate of the corrosion products was lower than the evaporation rate of NaCl. Viewed from Figures 3B, C, the mass of the corroded coatings kept increasing at 600°C and 700°C, and the final mass gains of the coatings were proportional to the testing temperature. Compared to the substrates, both NiSiAlY coatings

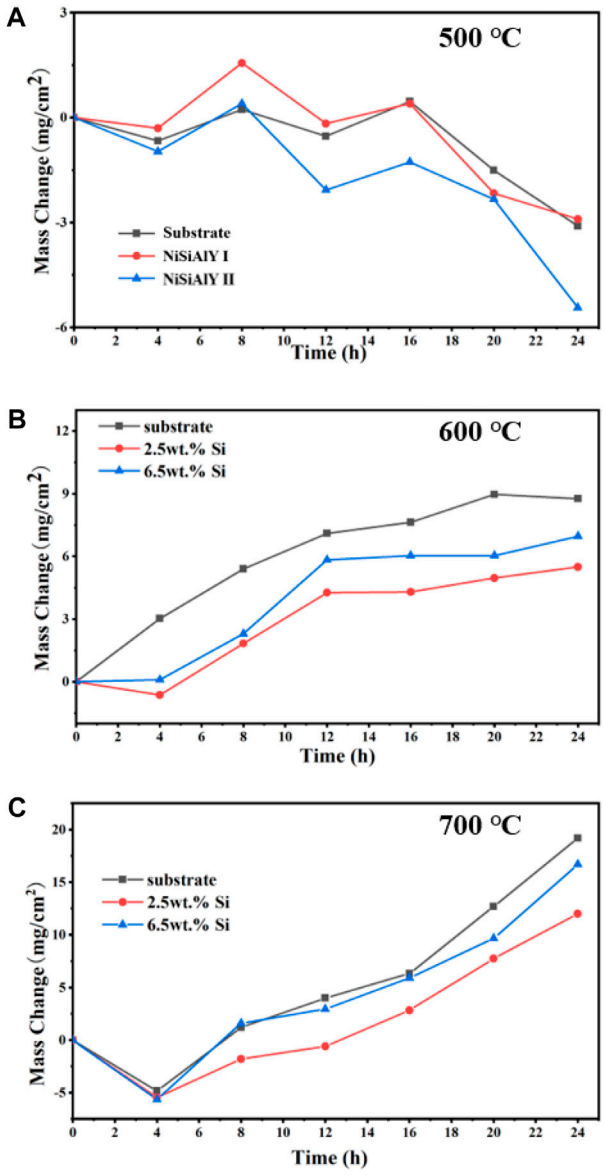

FIGURE 3
Corrosion kinetic curves of the NiSiAlY coatings and substrates at **(A)** 500°C, **(B)** 600°C, and **(C)** 700°C.

had slower mass growth during the hot corrosion tests at all temperatures. The NiSiAlY coatings exhibited effective corrosion resistance and protected capability. For the NiSiAlY Ⅰ, the final mass gain after the hot corrosion tests at 600°C and 700°C were 5.6 and 12 mg/cm^2. These values were less than that of the NiSiAlY Ⅱ (6.9 and 16.7 mg/cm^2). Obviously, the NiSiAlY Ⅰ showed the best resistance to the NaCl-induced hot corrosion.

XRD patterns of the NiSiAlY coatings after hot corrosion tests at 500, 600°C and 700°C are illustrated in Figure 4. Corrosion products including Al_2O_3 (PDF#10–0170), NiO (PDF#44–1159) and Na_2CrO_4 (PDF#25–1107) were detected on all the corroded coatings. Besides, the peaks of Al_2O_3 were very intensive, revealing that the oxide scales mainly consisted of Al_2O_3. According to the diffraction peaks, it could be noticed that more NiO formed on the surface of the NiSiAlY Ⅱ than the NiSiAlY Ⅰ. The content of Si seemed to have a certain influence on the formation of corrosion products during the NaCl-induced hot corrosion.

The surface morphologies of the NiSiAlY coatings with 2.5 wt% and 6.5 wt% Si after corrosion at different temperatures are presented in Figure 5. By comparison, Figures 5A, B showed that the oxide scales formed on the surface of the NiSiAlY coatings had more compact and smoother morphologies after the corrosion test at 500°C, indicating a lower corrosion rate caused by the relatively low temperature. In addition, the NiSiAlY Ⅱ exhibited a coarser surface morphology than the NiSiAlY Ⅰ. The corrosion on the surface seemed to be further accelerated with the higher content of Si. With the increase of corrosion temperature (600°C and 700°C), more corrosion products were intuitively observed on the surface of the NiSiAlY coatings. Both NiSiAlY coatings appeared coarse, uncompact and porous surfaces. Obviously, the higher corrosion temperature intensified the reaction between metallic elements and corrosion mediums.

Figure 6 displays the cross-sectional microstructures of the NiSiAlY coatings with 2.5 wt% and 6.5 wt% Si after the hot corrosion tests at different temperatures, the microstructures of the coatings showed significant differences. As shown in Figures 6A, B, oxide scale of the NiSiAlY Ⅱ was thicker than that of the NiSiAlY Ⅰ, and voids were found forming in it. However, no obvious internal corrosion and defects can be observed from the two coatings. Both NiSiAlY coatings exhibited good corrosion resistance at 500°C. At 600°C, the cross-sectional microstructures showed that both coatings suffered severer corrosion (Figures 6C, D). Viewed from Figure 6C, voids appeared in the oxide scale of the NiSiAlY Ⅰ. Nevertheless, the oxide scale formed on the surface exhibited continuous and dense structure. The coating still played an effective protective role in the corrosion process. With more content of Si, the NiSiAlY Ⅱ was severely corroded, and internal oxides were obviously observed beneath the coating (Figure 6D). Obviously, the coating cannot provide effective protection for the substrate, it showed poorer resistance to the NaCl-induced hot corrosion than the NiSiAlY Ⅰ. With a further increase of the corrosion temperature, a heavier hot corrosion was observed from both tested samples. Figure 6E showed that the oxide scale formed on the surface of the NiSiAlY Ⅰ became thicker, and the coating interior was obviously observed to be corroded. Not only that, slight internal corrosion was also found in the substrate. As shown in Figure 6F, the NiSiAlY Ⅱ suffered a severer corrosion at 700°C. Besides, it can be noted that a large area of internal corrosion formed beneath the coating accompanied with voids. Obviously, testing temperature and the Si content had significant effects on the corrosion behaviors of coatings. In addition, excess addition of Si in the NiSiAlY coatings could cause a negative influence, resulting in a worse corrosion resistance of the NiSiAlY Ⅱ to NaCl at elevated temperatures.

4 Discussion

Compared to oxidation, NaCl introduced hot corrosion can lead to a faster and heavier degradation of the coating. It has been widely recognized that NaCl played a critical role in the hot corrosion of coating in a marine service environment. Besides, water vapor might

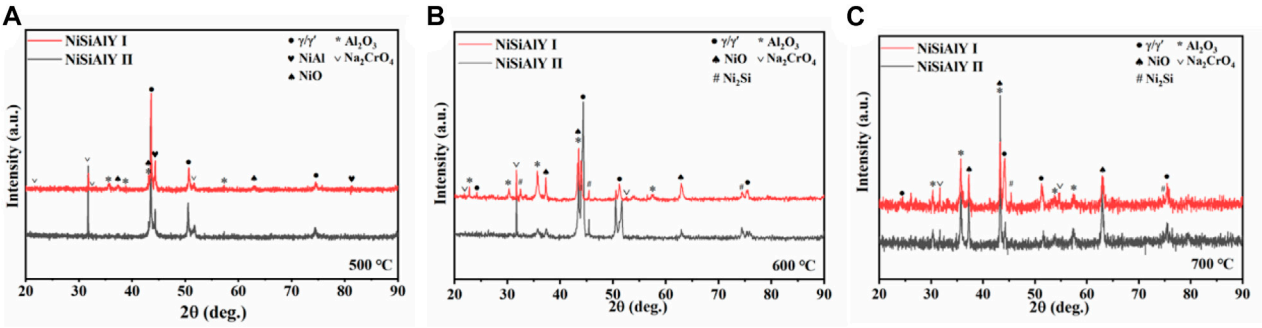

FIGURE 4
XRD patterns of the NiSiAlY I and NiSiAlY II after being corroded at **(A)** 500°C, **(B)** 600°C, and **(C)** 700°C.

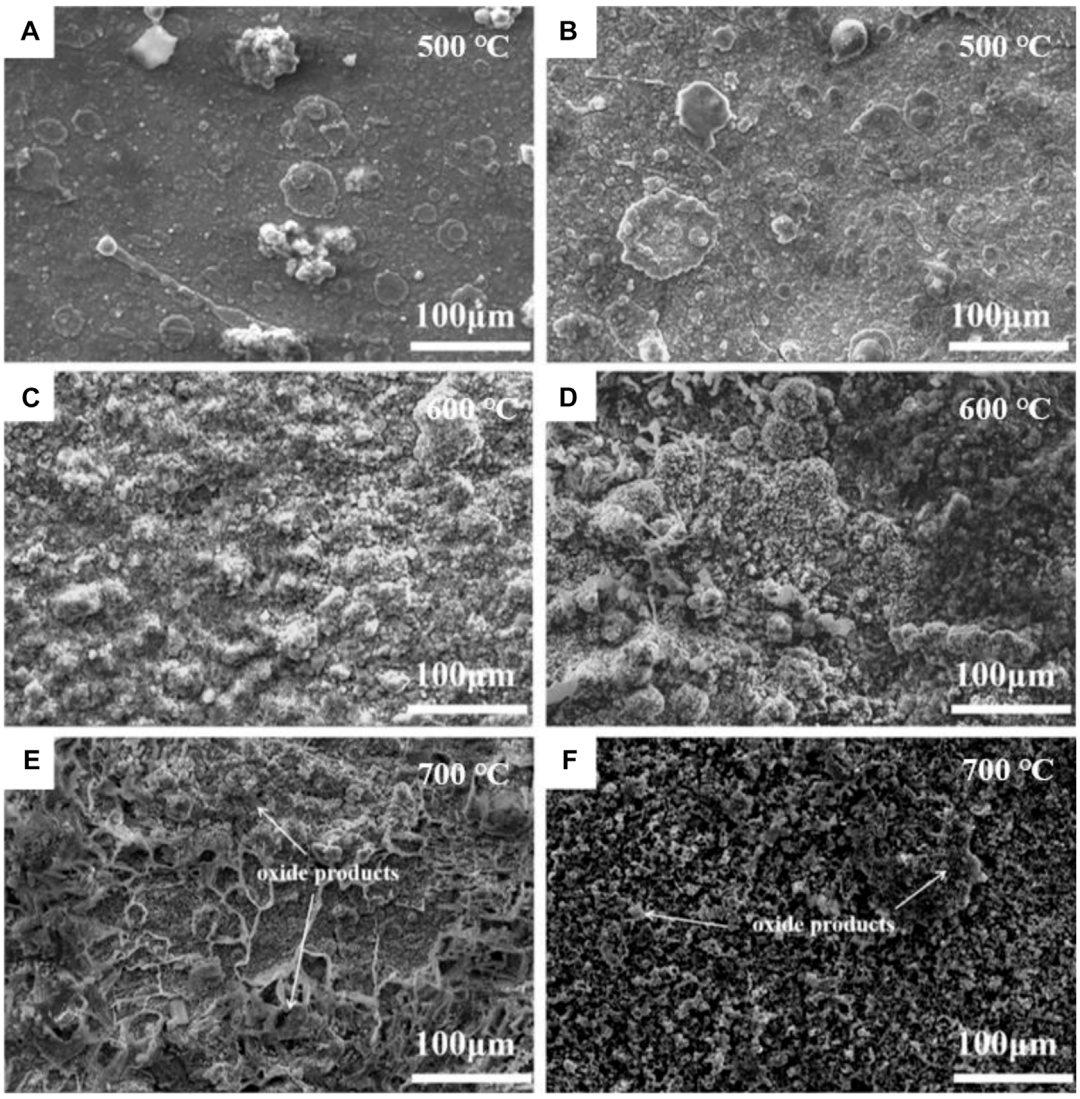

FIGURE 5
Surface morphology of the NiSiAlY coatings after corrosion test at different temperatures: **(A)** the NiSiAlY I at 500°C, **(B)** the NiSiAlY II at 500°C, **(C)** the NiSiAlY I at 600°C, **(D)** the NiSiAlY II at 600°C, **(E)** the NiSiAlY I at 700°C, **(F)** the NiSiAlY II at 700°C.

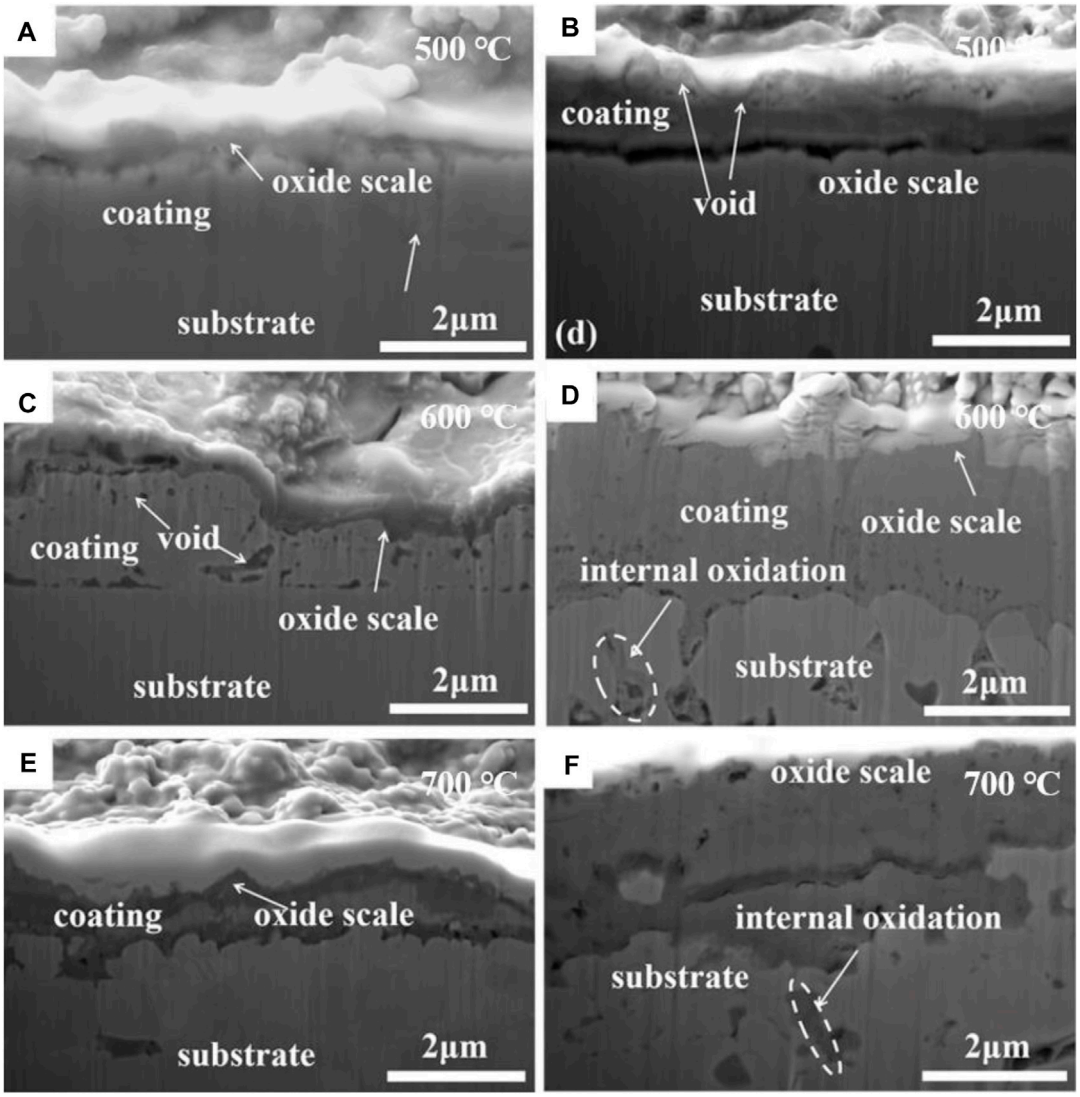

FIGURE 6
Cross-sectional microstructures of the NiSiAlY coatings after corrosion test at different temperatures: **(A)** the NiSiAlY I at 500°C, **(B)** the NiSiAlY II at 500°C, **(C)** the NiSiAlY I at 600°C, **(D)** the NiSiAlY II at 600°C, **(E)** the NiSiAlY I at 700°C, **(F)** the NiSiAlY II at 700°C.

dissociate into free H atoms and OH groups at elevated temperatures, further accelerating the chemical reactions on the surface (Douglass et al., 1996). In this study, the corrosion temperatures (500°C, 600°C, and 700°C) were lower than the melting point of NaCl (801°C). NaCl thus reacted with coating elements in the form of solid particles. The corrosion thus belonged to type II hot corrosion. According to the activity and content of relevant elements, the oxychlorination of Al was the main reaction from direct contact of the coatings and NaCl at the initial stage of corrosion, as listed below (Wang et al., 2022):

$$Al_{(s)} + 2NaCl_{(s)} + 5/2O_{2(g)} \rightarrow 1/2Al_2O_{3(s)} + Na_2O_{(s)} + 1/2Cl_{2(g)} \quad (2)$$

$$Al_{(s)} + NaCl_{(s)} + 3/4O_{2(g)} + H_2O_{(g)} \rightarrow 1/2Al_2O_{3(s)} + NaOH_{(g)} + HCl_{(g)} \quad (3)$$

Therefore, Al was quickly consumed under the synergistic effect of NaCl and water vapor on the surface, releasing corrosive gaseous Cl_2 and HCl [reactions (2) and (3)]. Meanwhile, part of the generated Cl_2 and HCl would diffuse into the coating/oxide interface through the defects or grain boundaries, further corroding the metal elements as described in reactions (4) and (5). Then, the volatile metal chlorides could diffuse outward and be rapidly oxidized by O_2 to form stable metal oxides with the following reactions (6) and (7). The corrosive Cl_2 and HCl were released again, continuing to participate in the hot corrosion. During the entire corrosion tests, Cl_2 and HCl were not be consumed by participating in the reactions. They acted as catalysts, constantly attacking the coatings. Furthermore, violent reactions would lead to the formation of large amounts of corrosion products, enhancing the internal stress of the oxide scale. Besides, the volatile substances such as Cl_2, HCl and $AlCl_3$ could destroy the integrity of the oxide scale in the process of overflow, resulting in a

TABLE 4 Standard Gibbs free energy of possible reactions at 500°C, 600°C and 700°C.

Possible reaction	ΔG (500°C/600°C/700°C, kJ/mol)
$2Ni_{(s)} + 4NaCl_{(s)} + O_{2(g)} \rightarrow 1/2NiCl_{2(g)} + Na_2O_{(s)}$	529.1/513.0/497.2
$Ni_{(s)} + 4NaCl_{(s)} + O_{2(g)} \rightarrow NiO_{(S)} + Na_2O_{(s)} + Cl_{2(g)}$	201.2/205.6/210.1
$2Ni_{(s)} + 2NaCl_{(s)} + 2H_2O_{(g)} \rightarrow 2NiCl_{(g)} + 2NaOH_{(l)} + Cl_{2(g)}$	201.2/205.6/210.1
$Ni_{(s)} + H_2O_{(g)} + O_{2(g)} \rightarrow NiO_{(S)} + H_{2(g)}$	36.6/40.0/43.3
$Ni_{(s)} + O_{2(g)} \rightarrow NiO_{(S)}$	−336.9/−319.3/−301.8

porous structure. The coatings were severely corroded with NaCl in a moist environment, and a higher service temperature can significantly accelerate the hot corrosion rate.

$$2M_{(s)} + xCl_{2(g)} \rightarrow 2MCl_{x(g)} \quad (4)$$

$$2M_{(s)} + 2xHCl_{(g)} \rightarrow 2MCl_{x(s)} + xH_{2(g)} \quad (5)$$

$$2MCl_{x(s)} + O_{2(g)} \rightarrow 2MO_{(s)} + xCl_{2(g)} \quad (6)$$

$$MCl_{(g)} + xH_2O_{(g)} \rightarrow MO_{x(s)} + 2xHCl_{(g)} \quad (7)$$

Based on the XRD patterns of the NiSiAlY alloys, intensive diffraction peaks of NiO were observed after hot corrosion tests at different temperatures (Figure 4). Obviously, the oxide scales formed on the surface contained lots of nickel oxide. NiO has a rock salt structure. Oxide scales which are composed of NiO generally exhibit a loose and porous microstructure. The such porous microstructure was beneficial for the inward infiltration of the corrosive mediums, leading to an accelerated corrosion rate. This seriously reduced the oxidation resistance of the alloy. In addition, the Pilling-Bedworth ratio (PBR) of the NiO (1.65) is higher than Al_2O_3 (1.28). The continuous accumulation of NiO could thus increase the internal stress of the oxide scale, finally leading to the peeling of the oxide scale. In order to promote the corrosion resistance of the coatings, it is particularly important to restrain the formation of NiO in the early stage of the corrosion. Through thermodynamic calculation, possible corrosion reactions of Ni exhibit positive standard Gibbs free energy, indicating that the corrosion of Ni was hard to react spontaneously with the solid NaCl particles and H_2O (Table 4). Ni accordingly only underwent oxidation reaction in the presence of NaCl during the initial stage. Generally, enhancing the content of Al in the Ni-Al binary alloy is widely used to reduce the selective oxidation of Ni and promote the formation of Al_2O_3. However, the content of Al in the coatings was limited since that the excessive addition of Al in coatings would have negative effects on the mechanical properties. Thus, enhancing the oxygen affinity of Al by doping elements to facilitate the formation of Al_2O_3 was vitally important. According to the third-element effect, the doping elements whose oxygen affinities are between the basis metal Ni and the protective oxide-forming element Al could promote the selective oxidation of Al, helping establish the protective scales on the surface (Niu et al., 2006). As shown in Figure 7, the Ellingham diagram of the possible oxidation reaction is presented. The stability of the oxides increases in the order of NiO, SiO_2, Al_2O_3 and Y_2O_3. Correspondingly, the sequence of oxygen affinity could be as follows: Y > Al > Si > Ni. Si, as one of the reactive elements, could thus make a third-element effect. Wagner proposed that the doped elements which conform to

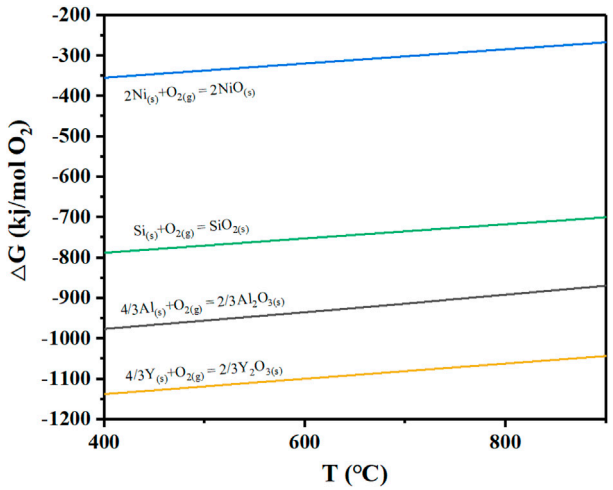

FIGURE 7
Ellingham diagram for possible oxidation products of the NiSiAlY coatings.

the third-element effect could tend to act as an oxygen getter to promote the oxidation of Al, restraining the formation of NiO. Therefore, Si could play a positive role in the high-temperature protection performance of the NiSiAlY coatings.

According to the XRD patterns of the coatings after the corrosion test at 600°C and 700°C, the characteristic peaks of the NiAl phase which were identified on the as-deposited coatings disappeared. This was attributed to the intensive consumption of Al during the NaCl-induced hot corrosion test, leading to the reduction of the Al-rich phase (Reaction 8). Al_2O_3 was accordingly formed on the surface.

$$3\beta - NiAl + 2NaCl + 2O_2 \rightarrow \gamma' - Ni_3Al + Al_2O_3 + Cl_2 + Na_2O \quad (8)$$

It is well accepted that the type of Al_2O_3 played an important role in the investigation of corrosion behaviors. It indicates the difference in the formational mechanism, growth rate and protection ability of the oxide scales. In order to confirm the type of Al_2O_3 formed on the surface of the coatings with 2.5 wt% and 6.5 wt% Si, the Photoluminescence (PL) was used to detect the relative contents of θ-Al_2O_3. The PL patterns of the samples with 2.5 wt% and 6.5 wt% Si are given in Figure 8. It is well known that the doublet peaks of α-Al_2O_3 appear at 14,432 and 14,402 cm^{-1} in a stress-free condition, while that of the θ-Al_2O_3 is at 14,645 and

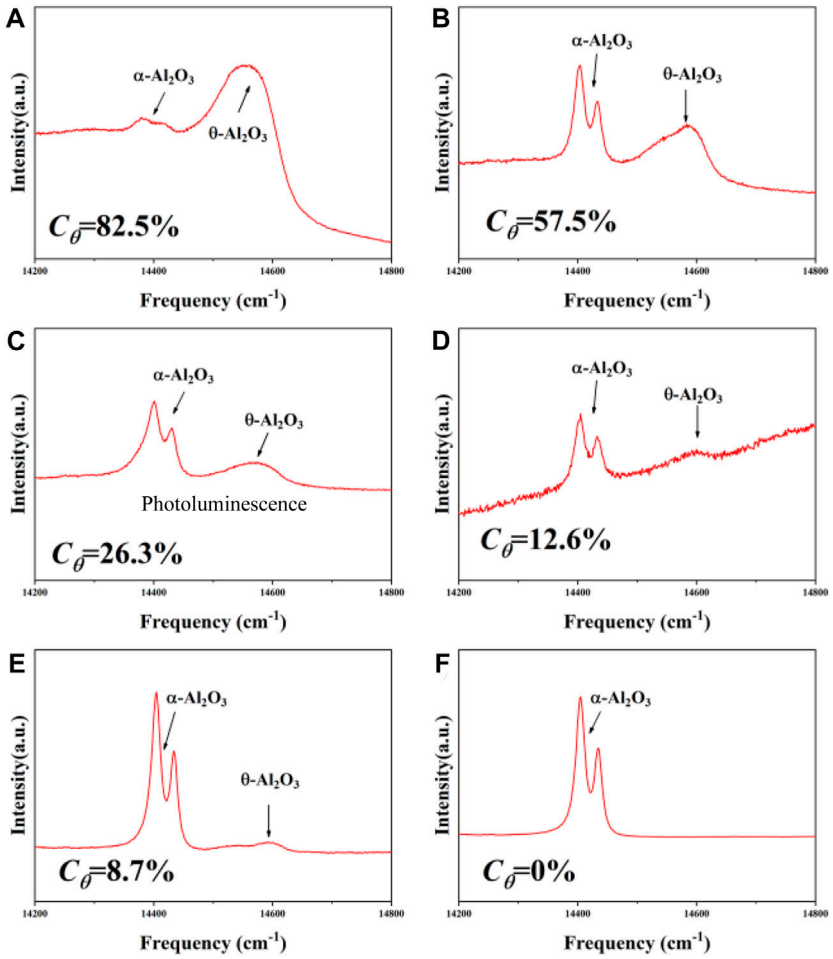

FIGURE 8
Photoluminescence (PL) patterns of the coatings after corrosion test at different temperatures: **(A)** the NiSiAlY I at 500°C, **(B)** the NiSiAlY II at 500°C, **(C)** the NiSiAlY I at 600°C, **(D)** the NiSiAlY II at 600°C, **(E)** the NiSiAlY I at 700°C, **(F)** the NiSiAlY II at 700°C.

14,575 cm^{-1}. The content of θ-Al_2O_3, $C_θ$, in the Al_2O_3 scale can be roughly estimated using the following relationship as listed in Eq. 9 (Chen et al., 2018).

$$C_\theta = \frac{A_{14575} + A_{14645}}{A_{14575} + A_{14402} + A_{14645} + A_{14432}} \quad (9)$$

in which A denoted the areas of the characteristic peaks. Based on the relative area of the Al_2O_3 peaks, the $C_θ$ of the NiSiAlY I was higher than that of the NiSiAlY II. It indicated that more α-Al_2O_3 was formed on the surface of the NiSiAlY II. Generally, in the oxidation process, the newborn Al_2O_3 from the reaction of Al and O_2 is mainly θ-Al_2O_3. In contrast, the corrosion product of Al in the NaCl-induced hot corrosion was generated in the form of α-Al_2O_3 (Cui et al., 2021). Therefore, higher proportion of α-Al_2O_3 indicated more intensive corrosion reactions on the surface of the NiSiAlY II. The consumption of Al was correspondingly accelerated. Moreover, the oxide scales formed by in the NaCl-induced hot corrosion were uncompact and porous, which was difficult to play a protective role. Furthermore, the priority depletion of Al would lead to rapid failure of the coatings in long-term corrosion. Moreover, with the consumption of Al, the Ni_2Si phase gradually formed in the coatings. During the intensive hot corrosion tests, the brittleness of the Ni_2Si phase would promote the inward diffusion of corrosive mediums, damaging the protection of the coatings (Yu et al., 2021).

5 Conclusion

In this paper, the NiSiAlY coatings with different Si contents were successfully prepared by arc-ion plating on the GH4169 substrate. The coatings mainly consisted of γ'-Ni_3Al with a limited amount of β-NiAl. During the hot corrosion tests at 500°C, 600°C, and 700°C, NaCl significantly accelerated the corrosion rate of all the coatings. The corrosion rate enhanced with increase of the temperature. For the NiSiAlY coatings, it exhibited effective high-temperature protection capability. Si could enhance the oxygen affinity of Al, promoting the formation of Al_2O_3 in the initial stage of corrosion. In addition, Si would accelerate the diffusion rate of Al in the coatings, leading to a rapid corrosion rate. Meanwhile, the Ni_2Si phase gradually formed with the consumption of Al, resulting in severe corrosion. Therefore, excess Si will reduce the corrosion resistance of the coatings.

Data availability statement

The original contributions presented in the study are included in the article/Supplementary Material, further inquiries can be directed to the corresponding authors.

Author contributions

MY: formal analysis, investigation, data curation, writing—original draft. DZ: conceptualization, methodology, writing—review and editing. BZ: conceptualization, visualization. YL: review and editing. YW: conceptualization.

Funding

This research was supported by the Jilin Province Science and Technology Development Plan (Grant No. YDZJ202301ZYTS285), the National Science Foundation for Young Scientists of China (Grant No. 52005490), the National Key R&D Program of China (Grant No. 2020YFB2010401) and the Innovation capacity building Foundation of Jilin Provincial Development and Reform Commission (Grant No. 2021C038-7).

Conflict of interest

The authors declare that the research was conducted in the absence of any commercial or financial relationships that could be construed as a potential conflict of interest.

Publisher's note

All claims expressed in this article are solely those of the authors and do not necessarily represent those of their affiliated organizations, or those of the publisher, the editors and the reviewers. Any product that may be evaluated in this article, or claim that may be made by its manufacturer, is not guaranteed or endorsed by the publisher.

References

Candan, S., and Bilgic, E. (2004). Corrosion behavior of Al–60 vol.% SiCp composites in NaCl solution. *Mater. Lett.* 58 (22-23), 2787–2790. doi:10.1016/j.matlet.2004.04.009

Chen, Y., Zhao, X., and Xiao, P. (2018). Effect of microstructure on early oxidation of MCrAlY coatings. *Acta Mater.* 159, 150–162. doi:10.1016/j.actamat.2018.08.018

Cui, T., Leng, W., Zhou, D., Yu, M., Wang, L., Li, J., et al. (2021). Improved hot corrosion resistance of Al-gradient NiSiAlY coatings at 750 °C by pre-oxidation. *Surf. Coatings Technol.* 417, 127187. doi:10.1016/j.surfcoat.2021.127187

Douglass, D. L., Kofstad, P., Rahmel, P., and Wood, G. (1996). International workshop on high-temperature corrosion. *Oxid. Metals* 45 (5-6), 529–620. doi:10.1007/BF01046850

Gurrappa, I. (1999). Hot corrosion behavior of CM 247 LC alloy in Na_2SO_4 and NaCl environments. *Oxid. Metals* 51 (5-6), 353–382. doi:10.1023/A:1018831025272

He, J., Luan, Y., Guo, H., Peng, H., Zhang, Y., Zhang, T., et al. (2013). The role of Cr and Si in affecting high-temperature oxidation behaviour of minor Dy doped NiAl alloys. *Corros. Sci.* 77, 322–333. doi:10.1016/j.corsci.2013.08.020

Hou, G., An, Y., Zhao, X., Zhou, H., and Chen, J. (2015). Effect of alumina dispersion on oxidation behavior as well as friction and wear behavior of HVOF-sprayed CoCrAlYTaCSi coating at elevated temperature up to 1000 °C. *Acta Mater.* 95, 164–175. doi:10.1016/j.actamat.2015.05.025

Li, R., Wang, S., Pu, J., Zhou, D., Yu, M., Wei, Y., et al. (2021). Study of NaCl-induced hot-corrosion behavior of TiN single-layer and TiN/Ti multilayer coatings at 500° C. *Corros. Sci.* 192, 109838. doi:10.1016/j.corsci.2021.109838

Li, W., Li, Y., Wang, Q., Sun, C., and Jiang, X. (2010). Oxidation of a NiCrAlYSi overlayer with or without a diffusion barrier deposited by one-step arc ion plating. *Corros. Sci.* 52 (5), 1753–1761. doi:10.1016/j.corsci.2010.02.022

Liu, Z., Shen, M., Zhu, S., Huang, Y., Ma, W., Jia, Y., et al. (2020). Effect of nitrogen content on the phase transformation of alumina scale on a nanocrystalline NiCrAlYSiHfN/AlN multilayer coating. *Corros. Sci.* 165, 108396. doi:10.1016/j.corsci.2019.108396

Ma, J., Jiang, S. M., Gong, J., and Sun, C. (2013). Hot corrosion properties of composite coatings in the presence of NaCl at 700 and 900°C. *Corros. Sci.* 70, 29–36. doi:10.1016/j.corsci.2013.01.004

Niu, Y., Zhang, X. J., Wu, Y., and Gesmundo, F. (2006). The third-element effect in the oxidation of Ni–Cr–7Al (= 0, 5, 10, 15 at.%) alloys in 1 atm O_2 at 900–1000 °C. *Corros. Sci.* 48 (12), 4020–4036. doi:10.1016/j.corsci.2006.03.008

Norrell, T., Ferguson, G., Ansell, T., Saladin, T., Nardi, A., and Nieto, A. (2020). Synthesis and corrosion behavior of cold sprayed dual nanoparticle reinforced Al coatings. *Surf. Coatings Technol.* 401, 126280. doi:10.1016/j.surfcoat.2020.126280

Peng, X., Xia, C., Dai, X., Wu, A., Dong, L., Li, D., et al. (2013). Study on the interface reaction behavior of NiCrAlY coating on titanium alloy. *Surf. Coatings Technol.* 232, 254–263. doi:10.1016/j.surfcoat.2013.05.024

Qi, J., Wang, L., Hao, J., Zhang, Y., He, X., Pang, H., et al. (2023). Self-adaptive root-like capillary diffusion channels enabled by TaN/Zr3N4 nanomultilayered architecture: Achieving superior corrosion resistance. *Mater. Desigin* 225, 111555. doi:10.1016/j.matdes.2022.111555

Ren, X., Wang, F., and Wang, X. (2005). High-temperature oxidation and hot corrosion behaviors of the NiCr–CrAl coating on a nickel-based superalloy. *Surf. coatings Technol.* 198 (1-3), 425–431. doi:10.1016/j.surfcoat.2004.10.108

Sadeghimeresht, E., Eklund, J., Phother Simon, J., Liske, J., Markocsan, N., and Joshi, S. (2018). Effect of water vapor on the oxidation behavior of HVAF-sprayed NiCr and NiCrAlY coatings. *Mater. Corros.* 69 (10), 1431–1440. doi:10.1002/maco.201710005

Saharkhiz, R., Valefi, Z., Mirjani, M., Abdollahi, A., and Taghi-Ramezani, S. (2020). Effect of hydrogen and argon shrouding gas flow rate on high-temperature oxidation behavior of NiCrAlY coating by solid shielding shrouded plasma spray (SSPS). *Surf. Coatings Technol.* 394, 125818. doi:10.1016/j.surfcoat.2020.125818

Shinata, Y., and Nishi, Y. (1986). NaCl-induced accelerated oxidation of chromium. *Oxid. metals* 26 (3-4), 201–212. doi:10.1007/BF00659184

Shu, Y., Wang, F., and Wu, W. (2000). Corrosion behavior of pure Cr with a solid NaCl deposit in O_2 plus water vapor. *Oxid. Metals* 54 (5-6), 457–471. doi:10.1023/A:1004690518225

Sun, Y., Xu, S., and Shan, A. (2015). Effects of annealing on microstructure and mechanical properties of nano-grained Ni-based alloy produced by severe cold rolling. *Mater. Sci. Eng. A* 641, 181–188. doi:10.1016/j.msea.2015.06.043

Texier, D., Copin, E., Flores, A., Lee, J., Terner, M., Hong, H., et al. (2020). High temperature oxidation of NiCrAlY coated Alloy 625 manufactured by selective laser melting. *Surf. Coatings Technol.* 398, 126041. doi:10.1016/j.surfcoat.2020.126041

Tsaur, C. C., Rock, J. C., Wang, C. J., and Su, Y. (2005). The hot corrosion of 310 stainless steel with pre-coated NaCl/Na_2SO_4 mixtures at 750 °C. *Mater. Chem. Phys.* 89, 445–453. doi:10.1016/j.matchemphys.2004.10.002

Wang, B., Gong, J., Sun, C., Huang, R., and Wen, L. (2003). The behavior of MCrAlY coatings on Ni_3Al-base superalloy. *Mater. Sci. Eng. A* 357 (1-2), 39–44. doi:10.1016/S0921-5093(03)00254-5

Wang, C., Jiang, F., and Wang, F. (2004). Corrosion inhibition of 304 stainless steel by nano-sized Ti/silicone coatings in an environment containing NaCl and water vapor at 400–600 °C. *Oxid. metals* 62 (1-2), 1–13. doi:10.1023/B:OXID.0000038782.77162.5b

Wang, F., Shu, Y., Lu, D. r., Xue, J. l., and Zhang, X. (2003). Influence of Cr content on the corrosion of Fe–Cr alloys: The synergistic effect of NaCl and water vapor. *Oxid. Metals* 59 (3-4), 201–205. doi:10.1023/A:1023083309041

Wang, H., Zuo, D., Gang, C., Sun, G., Li, X., and Xu, C. (2010). Hot corrosion behaviour of low Al NiCoCrAlY cladded coatings reinforced by nano-particles on a Ni-base super alloy. *Corros. Sci.* 52 (10), 3561–3567. doi:10.1016/j.corsci.2010.07.011

Wang, Q., Zhou, D., Yu, M., Shi, L., and Sun, Q. (2022). Oxidation and hot corrosion behaviors of Mo-doped NiMoAlY alloys at 750 °C. *Corros. Sci.* 201 (108–109), 110262. doi:10.1016/j.corsci.2022.110262

Wu, J., Yang, W., Zhang, X., Wang, C., Zhuo, X., Zhan, Y., et al. (2023). Corrosion behavior of PS-PVD spray Yb2Si2O7 environmental barrier coatings during continuous water vapor exposure. *Corros. Sci.* 210, 110831. doi:10.1016/j.corsci.2022.110831

Wu, L., Osada, T., Watanabe, I., Yokokawa, T., Kobayashi, T., and Kawagishi, K. (2021). Strength prediction of Ni-base disc superalloys: Modified γ′ hardening models applicable to commercial alloys. *Mater. Sci. Eng. A* 799, 140103. doi:10.1016/j.msea.2020.140103

Wu, Y., Qin, X., Wang, C., and Zhou, L. (2019). Influence of phosphorus on hot deformation microstructure of a Ni-Fe-Cr based alloy. *Mater. Sci. Eng. A* 768, 138454. doi:10.1016/j.msea.2019.138454

Xing, Y. Y., Dai, B., Wei, X. H., Ma, Y. J., and Wang, M. (2014). Enhancement of high-temperature oxidation resistance and mechanical properties of Ni_3Al thin films by inserting ultrathin Cr layers. *Vacuum* 101, 107–112. doi:10.1016/j.vacuum.2013.07.040

Xu, C., and Gao, W. (2000). Pilling-Bedworth ratio for oxidation of alloys. *Material Res. Innovations* 3 (4), 231–235. doi:10.1007/s100190050008

Yang, Y. F., Ren, P., Bao, Z. B., Zhu, S. L., Wang, F. H., and Li, W. (2020). Effect of Pt-rich position on the hot corrosion behavior of NiCoCrAlY coating for a single-crystal superalloy. *Surf. Coatings Technol.* 395, 125938. doi:10.1016/j.surfcoat.2020.125938

Yu, M., Cui, T., Zhou, D., Li, R., Pu, J., and Li, C. (2021). Improved oxidation and hot corrosion resistance of the NiSiAlY alloy at 750 ℃. *Mater. Commun.* 29, 102939. doi:10.1016/j.mtcomm.2021.102939

Yu, M., Sun, Q., Wang, Q., Li, X., Zhou, D., Pu, J., et al. (2022). Effect of Pt-doping on the oxidation behaviors of the γ'-Ni_3Al and β-NiAl phases in the NiSiAlY alloy. *Corros. Sci.* 200, 110224. doi:10.1016/j.corsci.2022.110224

Zhang, X., Deng, Z., Li, H., Mao, J., Deng, C., Deng, C., et al. (2020). Al_2O_3-modified PS-PVD 7YSZ thermal barrier coatings for advanced gas-turbine engines. *Mater. Degrad.* 4 (1), 31. doi:10.1038/s41529-020-00134-5

Zhang, Z., Hosoda, S., Kim, I.-S., and Watanabe, Y. (2006). Grain refining performance for Al and Al–Si alloy casts by addition of equal-channel angular pressed Al–5mass% Ti alloy. *Mater. Sci. Eng. A* 425 (1), 55–63. doi:10.1016/j.msea.2006.03.018